



Extreme gas production in anthropogenic fibrous sediments: An overlooked biogenic source of greenhouse gas emissions



Alizée P. Lehoux^{a,*}, Anastasija Isidorova^b, Fredrik Collin^a, John Koestel^{c,d}, Ian Snowball^a, Anna-Karin Dahlberg^e

^a Department of Earth Sciences, Natural Resources and Sustainable Development, Uppsala University, Villavägen 16, SE-751 36 Uppsala, Sweden

^b Department of Ecology and Genetics, Limnology, Uppsala University, Norbyvägen 18 D, SE-752 36 Uppsala, Sweden

^c Department of Soil and Environment, Swedish University of Agricultural Sciences, Box 7014, SE-750 07 Uppsala, Sweden

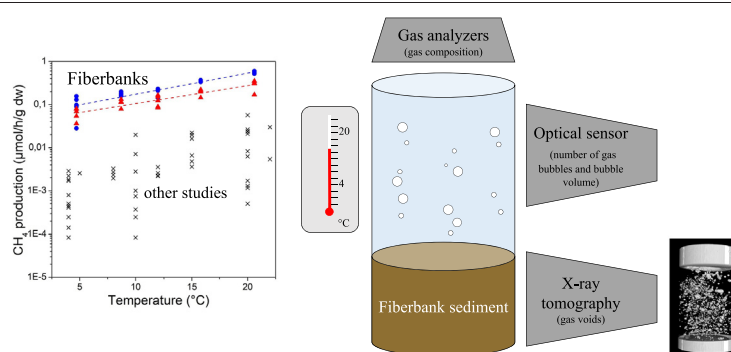
^d Forschungsanstalt Agroscope Reckenholz-Tanikon, Reckenholzstrasse 191, 8046 Zürich, Switzerland

^e Department of Aquatic Sciences and Assessment, Swedish University of Agricultural Sciences, Box 7050, SE-750 07 Uppsala, Sweden

HIGHLIGHTS

- Fiberbanks are contaminated fibrous legacy sediments showing signs of gas release.
- Gas production and release were studied with tomography, optical sensors, gas analyzers.
- The released gas from fiberbanks is composed of greenhouse gases (CH₄ and CO₂).
- Fiberbanks' CH₄ production rates are much higher than reported rates from sediments.
- Fiberbanks might represent a significant source of greenhouse gases emissions.

GRAPHICAL ABSTRACT



ARTICLE INFO

Article history:

Received 9 January 2021

Received in revised form 20 March 2021

Accepted 22 March 2021

Available online 27 March 2021

Editor: Filip M.G. Tack

Keywords:

Contaminated sediment

Fiberbanks

Methane

Gas release

Paper industry

X-ray

ABSTRACT

Fibrous sediments that originated from old pulp and paper industry emissions are recognized as a potential threat to the aquatic environment because they are highly contaminated. In addition, biogenic degradation of the organic material from so-called "fiberbanks" has a high potential to produce greenhouse gases (GHG). In this study, X-ray tomography, optical sensors and gas analyzers were used to identify and quantify the gas produced and released from samples of two different fiberbanks. We show that a finer fibrous structure allows the formation of larger gas bubbles and higher gas production rates compared to coarser material composed of wood pieces. High contents of methane (average 56% to 65%) and carbon dioxide (average 18% to 20%) were measured in the gas emitted from both types of fiberbank. Measured methane production rates from the fiberbanks samples are one to three orders of magnitude higher than previously reported rates from sediments within the studied temperature range (between 0.03 and 0.51 μm CH₄/h/g dw over 4.7 to 20 °C). The potential for methane and carbon dioxide production in the fiberbank volume likely present in Sweden is estimated to correspond to 7% of Sweden's total known GHG emissions for 2019. These findings show that fiberbanks have the potential to be a significant emitter of GHG.

© 2021 The Author(s). Published by Elsevier B.V. This is an open access article under the CC BY license (<http://creativecommons.org/licenses/by/4.0/>).

1. Introduction

In recent years, a unique type of anthropogenic organic-rich sediment originating from old wastes from sawmills and the pulp and paper industry has received attention in Sweden (Norrlin and

* Corresponding author.

E-mail address: alizee.lehoux@geo.uu.se (A.P. Lehoux).

Josefsson, 2017; Apler et al., 2019; Apler et al., 2020; Dahlberg et al., 2020). Historically, these industries released large quantities of cellulose material with their untreated waste water (Ali and Sreerishnan, 2001). Some of this organic material accumulated close to the wastewater outlet and formed fiber-deposits (*fiberbanks*) that can be several meters thick in shallow coastal areas and lakes, while some of it was transported and deposited further away, forming fiber-rich sediments. Depending on the type of industrial process responsible for the emissions, the fibrous material in fiberbanks can consist of coarse wood material (centimeter large wood chips and wood shavings) or pulp cellulose fibers with a texture similar to cotton-wool. Although the discharge of untreated cellulose wastes into water bodies was banned in Sweden in 1969, these fibrous deposits still exist and are an unwanted legacy because they are contaminated by metals and persistent organic pollutants (POPs) (Norrlin and Josefsson, 2017; Apler et al., 2019; Dahlberg et al., 2020; Rodríguez et al., 2021). Similar fibrous deposits have been found in other countries (e.g. Finland (Kokko et al., 2018), Canada (Biberhofer et al., 2011) and USA (WSDE, 2012)).

Degradation of organic material under anaerobic conditions leads to biogenic production of methane (CH_4) and carbon dioxide (CO_2) in sediment via methanogenesis (Bastviken, 2009; Fenchel et al., 2012). Methane is a potent greenhouse gas (GHG), with 34 times higher global warming potential (GWP) than carbon dioxide, when considering a 100 years' timescale and including climate-carbon feedbacks (Myhre et al., 2013). The potential of sediment to produce CH_4 depends on several factors such as temperature (Bastviken, 2009; Berberich et al., 2020), and the quantity and quality of available organic matter. CH_4 released from natural sediment can be an important source of CH_4 to the atmosphere (Judd et al., 2002), and due to the fiberbank's high TOC values, their CH_4 emission may exceed that of natural sediment.

Gas bubble growth and migration has been studied in different types of natural sediments (van Kessel and van Kesteren, 2002; Gardiner et al., 2003; Liu et al., 2016; Johnson et al., 2017; Liu et al., 2018). Gas is released into sediment pores as a by-product of biodegradation and when the gas concentration in the sediment pore water reaches oversaturation, gas bubbles start to form. CH_4 is particularly prone to form gas bubbles due to its low solubility in water (van Kessel and van Kesteren, 2002). Slow diffusive transport combined with high gas production rates causes gas to accumulate in the sediment. When the gas partial pressure exceeds the atmospheric and hydrostatic pressure of the overlying water, the gas bubbles migrate upwards through the sediment and into the overlying water through ebullition (Bastviken et al., 2004; Scandella et al., 2011). The bubble growth inside the sediment can cause sediment fracturing and the formation of macropore networks that further serve as quasi-permanent channels for regular ebullition events (Liu et al., 2018). Gas ebullition can also enhance contaminant dispersal from sediments as the gas bubbles tend to gather hydrophobic and/or volatile contaminants from the pore water by gas/water partitioning (Fendinger et al., 1992). Others have also reported increased sediment pore-water exchange (Klein, 2006) and resuspension of contaminated particles during gas ebullition (Yuan et al., 2007; Viana et al., 2012).

A majority of the fiberbanks that have been surveyed in Sweden (76% or 22 of the 29 surveyed fiberbanks, including the ones sampled in this study) show signs of gas ebullition in the form of pockmarks on the sediment surface (Norrlin and Josefsson, 2017). Pockmarks form when gas bubbles protrude the sediment during release, and have shown persistent activity over the scale of days and even months (Scandella et al., 2017). The gas trapped inside the fiberbanks also gives rise to a characteristic hydroacoustic signal (Apler et al., 2014). Gas emissions from fiberbank sediments have not been studied despite their potential importance for contaminant dispersal and GHG emissions. CH_4 production in lake sediment has shown to increase significantly with temperature (Duc et al., 2010), and CH_4 fluxes have also shown consistent temperature dependence across microbial and ecosystem scales (Yvon-Durocher et al., 2014). Hence, there is a possibility

that increasing seasonal temperature variations, linked to climate change and its effects on local conditions, may enhance the gas production in fiberbanks.

In this study we investigated key characteristics of the gas formed and emitted from two different types of fiberbank sediments (which represent the two extreme types of surveyed fiberbanks in terms of texture, according to Norrlin and Josefsson (2017)), including gas composition, amount, and bubble evolution within the sediments, in order to evaluate the importance of this GHG source and the potential implications for contaminants transport. The two types of sediments consisted mainly either of soft cellulose wood fibers (Väja) or coarse wood chips (Sandviken). Bubble growth and bubble migration were studied using X-ray tomography, which enables 3D-imaging of gas voids inside the sediment and monitoring of bubble growth over time. Gas production, release and composition as a function of the temperature were determined using an optical sensor and gas analyzers in incubation experiments.

2. Material & methods

2.1. Fiberbank sediments sampling

Sediment samples were obtained from two fiberbanks located in the brackish Ångermanälven river estuary (Väja N 637814.0905, E 6985862.666 and Sandviken N 640790.26, E 6983664.56 in SWEREF99 TM system), in north eastern Sweden. Several pulp and paper mills were located in this area during the 19th and 20th centuries and several fiberbanks were found in surveys (Apler et al., 2014). The Väja fiberbank is located next to an active sulfate pulp mill that produces unbleached kraft pulp. The production of unbleached pulp at this industrial site started already in 1914/1915. The fiberbank in Väja covers approximately 70,000 m² with a sediment thickness of at least 6 m and consists mainly of cellulose fibers with a cotton-wool like texture. The fiberbank is located at a water depth of around 15 m and is permanently anoxic at the sediment surface (Apler et al., 2019). The Sandviken fiberbank is located next to an old kraft pulp mill that operated between 1907 and 1977, and was demolished in 1979. The fiberbank in Sandviken covers approximately 55,000 m² with a sediment thickness of around 6 m and consists mainly of several centimeter large wood chips. The fiberbank is located at a water depth of around 12 m and is permanently hypoxic (Apler et al., 2019).

Sediments from Väja and Sandviken fiberbanks were sampled in autumn 2018 from the Swedish Geological Survey's vessel Ocean Surveyor using sediment grab samplers (Orange Peel Bucket and Ekman). The sediments collected represent bulk fibrous material sampled from the upper 50 cm of each fiberbank since the sediment was too loose to recover intact sediment cores. The sediment samples were stored in plastic buckets in darkness at 4 °C. The sediment was homogenized before being used in the experiments described in the following sections. Field measurements showed a temperature of around 4–5 °C near the sediment surface. Although the sediment surface temperature most probably varies through the year, we incubated samples at this temperature in most of our experiments. Each experiment described below was conducted on new sediment samples.

2.2. Fiberbank sediment characterization

An aliquot of wet sediment was used to determine its dry weight and loss on ignition by heating the sample to 105 °C for 24 h and 550 °C for 4 h, respectively. In addition, the sediment content of total-carbon (TC), total organic carbon (TOC) and total-nitrogen (TN) were determined by dry combustion at 1350 °C and elementary analysis using a TruMac instrument (Leco Corporation, St Joseph, USA) following the Swedish Standard procedure SS-ISO 10694 at the Swedish University of Agricultural Sciences. Ethylenediaminetetraacetic acid (EDTA, Leco Corporation, St Joseph, USA) was used as a standard for calibration

(Carbon % 41.00 ± 0.15 , Nitrogen % 9.57 ± 0.04). A control sample was analyzed with every set of samples and showed a relative standard deviation (RSD) less than 2% for carbon.

2.3. Imaging of the gas voids within the sediments

A plexiglass column (25 cm height, 10 cm diameter) containing each sediment type was prepared with 650 g of wet Sandviken fiberbank sediment and 797 g of wet Våja fiberbank sediment, to reach the same height of the sediment column (10 cm). Tap water was poured onto the top of the sediment to create a 5 cm water column above the sediment surface, corresponding to 500 g in the Sandviken column and 376 g in the Våja column. The larger amount of water added to the Sandviken column is due to a much lower sediment water content. The columns were covered with a lid in order to limit evaporation, but not tightly sealed to allow the gas produced in the samples to escape.

Directly after their preparation, the columns were X-rayed using a GE Phoenix v|tome|x 240 XRT scanner with a tungsten target and a 16" flat panel detector with a four-megapixel resolution (GE DRX250RT). The X-ray tomography data were obtained using a voltage of 150 kV and an electrical current of 660 μ A. A copper filter of 0.2 mm thickness was used to reduce beam-hardening artifacts. Projections from 2000 angles were recorded whereas four radiographs were acquired per projection with an exposure time of 200 ms. The first radiograph was discarded to minimize afterglow effects of the detector crystals and the last three were averaged to reduce image noise. The image acquisition time for one sample was approximately 30 min. The projections were then reconstructed to a three-dimensional (3-D) image using the GE software datos 2.1. RTM. The voxel size was 90 μ m which means that structures larger than 180 μ m could be identified in the image.

The columns were then incubated in the dark at a temperature of 4 °C in order to simulate field conditions. Additional X-ray images were recorded after increasingly longer intervals over a total of 109 days. In total, each sample was X-rayed 10 times throughout the experiment.

The images were processed with the open-source software ImageJ (Schneider et al., 2012). The plugin Soijl was used for calibrating the

images to a common gray-scale as explained in Koestel (2018), thereby correcting illumination bias along the vertical direction. The gas bubbles were segmented using a global threshold, which was defined by the minimum in the image histogram between peaks corresponding to gas and liquid phases (minimum method). Resulting binary images were then analyzed with Soijl's implementation of BoneJ (Doube et al., 2010) and MorphoLibJ (Legland et al., 2016).

2.4. Characterization of gas bubbles released through ebullition

The number and size of gas bubbles released through ebullition were characterized using a custom-made optical sensor inspired by Delwiche et al. (Delwiche et al., 2015; Delwiche and Hemond, 2017). The sensor setup consists of an Arduino Nano Every 5 V 20 MHz logger, two infra-red-light emitting diodes (IR LEDs, Everlight IR928-6C-F 940 Nm) and two IR phototransistors (Everlight IR928-6C-F 940 Nm). The circuit diagram is presented in Fig. S1. The Arduino logger uses the IR phototransistors to sense the transmittance of IR light through a glass-funnel at two points separated by a known distance ($x = 12.8$ mm) (Fig. 1). Due to the much lower density of the ebullition gas compared to the water, bubbles passing the IR LEDs result in a substantial increase in light refraction. The increase in refraction causes a large drop in the IR transmittance to the IR phototransistor, allowing to log the time when the leading and trailing edge of a bubble passes both sets of LEDs.

The logger is programmed to use this information to calculate the bubble rise velocity and the time difference between the leading and trailing bubble edge, and with that infer the bubble length inside the funnel. The logger then calculates the bubble volume (V) using the inner cross-section area of the funnel stem ($a = 9.2$ mm²) as described in Eq. (1):

$$V = \frac{x}{t_0} \times dt \times a \quad (1)$$

where t_0 is the time difference between when the leading edge of the bubble passes the lower and the upper LEDs, and dt is the time difference between the leading and trailing bubble edge.

The Arduino logger was connected to a computer using a serial connection and the bubble characteristics were printed to the Arduino IDE

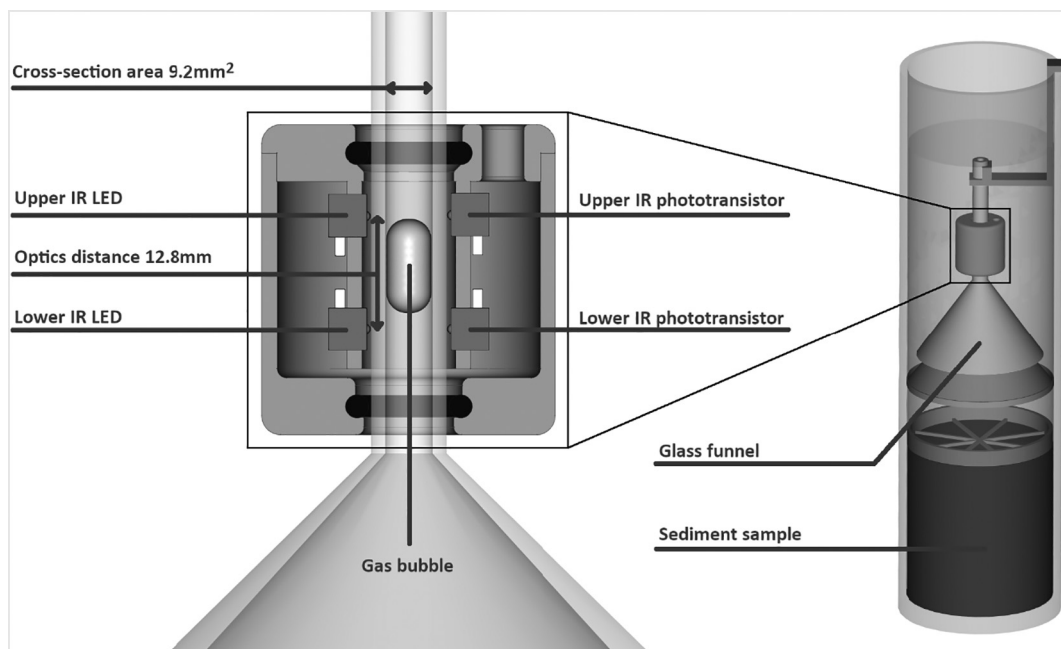


Fig. 1. Schematic view of the custom-made sensor with the two infra-red-light emitting diodes and the two IR phototransistors depicted.

serial monitor by the logger. The bubbles were then analyzed using Excel™ and MATLAB™ R2019b to determine the combined daily gas volume, the average bubble volume and the number of bubbles.

For the incubation experiments, two plexiglass columns (40 cm height, 10 cm diameter) were prepared with approximately 10 cm of homogenized sediment (one column for each sediment type) and 30 cm of artificial seawater (5‰ salinity). The optical sensor funnels were attached inside the columns, 15 cm above the sediment surface in such a way that they would catch and measure every released bubble (see Fig. 1). The entire setup was placed in an incubator set to 4 °C (9 days), 7 °C (19 days), 10 °C (18 days), 15 °C (10 days) and 20 °C (24 days). After reaching stable conditions, the sensor recordings for 5 continuous days were used for graphical presentations and statistical evaluation.

2.5. Gas composition

Homogenized fiberbank sediment from Vāja and Sandviken, respectively, was incubated in three columns (20 cm inner diameter, 90 cm high) with artificial seawater (salinity of 5‰ to simulate field conditions) at 20 °C in darkness. Approximately one liter of gas released through ebullition was collected in a gas sampling bag (Sigma-Aldrich, Saint-Louis, USA) attached to a funnel fixed in the water column above the sediment. The gas composition (CH₄, CO₂, O₂ and H₂S) was measured using a Biogas 5000 instrument (Geotechnical Instruments Ltd., Coventry, UK).

2.6. Methane production at various temperatures

Sub-samples of homogenized sediment (20 mL) from each site were transferred into pre-weighted 117 mL serum vials in a glove box (N₂ environment). The final weight of the wet sediment was approximately 22 g, which corresponded to 3.5–4 g of dry sediment. Five replicates from each site were prepared. The samples were sealed and flushed with N₂ after preparation. Samples were incubated anoxically in the dark at 4.7, 8.7, 12.0, 15.8 and 20.6 °C (target temperatures were 4, 8, 12, 16 and 20 °C but a variation was observed due to the experimental setup, and only recorded temperatures are considered further on). Prior to incubations, the samples were flushed with N₂ for at least 2 min and placed in a water bath in the dark at the incubation temperature for at least 1 day before starting the incubation to ensure stable conditions in the vials and allow time for removal of potential trace oxygen contamination. To measure initial gas concentration in the vials the samples were shaken for at least 1 min to allow the equilibration of CH₄ between the headspace and the pore-water. The pressure in the vials was measured with a needle barometer, and 1 mL of the sample was extracted with 1 mL syringe equipped with a stopcock. The samples were immediately injected into the Ultraportable Greenhouse Gas Analyzer (UGGA, Los Gatos Research, San Jose, USA) and gas

concentrations were quantified with an in-house R script (Team, 2017; Paranaiba et al., 2018). For calibration, different volumes of CH₄ standards (AGA) were injected into UGGA and the peaks area were integrated. Peak areas and the amount of gas (mols) were used for the linear calibration curves. Separate calibration curves were prepared for low (up to 0.21 μmol CH₄ ($r^2 = 0.99$, $n = 19$)) and high (0.21 to 1.69 μmol CH₄ ($r^2 = 0.99$, $n = 13$)) amounts of injected gas to achieve better precision for low concentrations. The samples were incubated for 2–3 days in the water bath at the specified temperature. To finish the incubations, the samples were shaken again for 1 min, the pressure inside the vials was measured, and 1 mL of headspace gas was extracted and immediately injected into the UGGA. The samples were then flushed with N₂ and the protocol was repeated for the next temperature. The measurements were repeated on the same samples (vials) at different temperatures. Samples were incubated at 4.7 °C (68 h), 8.7 °C (69 h), 12 °C (50 h), 15.8 °C (72 h), and 20.6 °C (48 h). The amount of CH₄ in the headspace in the vials was calculated according to the ideal gas law using CH₄ concentration obtained from UGGA, pressure in the bottles, gas volume and temperature of the vials. The CH₄ partitioning between the headspace and pore-water was calculated according to Henry's law (Weiss, 1974; Wiesenburg and Guinasso, 1979). The total amount of CH₄ in headspace and in porewater was divided by the dry weight of the material, and the rate was calculated as the difference between the initial and final CH₄ amount per dry weight per incubation time for incubations at each temperature.

2.7. Statistical analyses

Statistical analyses were performed using the statistical software Graph Pad Prism (Graph Pad Software Inc). Spearman rank correlation analysis and linear regression analysis were performed to test the relationship between gas production and temperature. Unpaired *t*-test was used to test for significant differences in gas production between Vāja and Sandviken.

3. Results and discussion

3.1. Formation of gas voids within the sediment

The X-ray measurements show that the average gas void volume (including only bubbles larger than 180 μm) increased with time in both types of sediment, whereas the number of gas voids decreased with time (Figs. 2 and 3), indicating that small gas voids merged to create larger voids and that some gas escaped from the sediment over time. An increase in average gas void volumes was measured during the experiment (109 days), without reaching a stable volume. A larger total gas volume was measured in the Sandviken column compared to the Vāja column and was distributed in fewer gas voids. An increase in total gas volume was observed in the Sandviken column, followed by

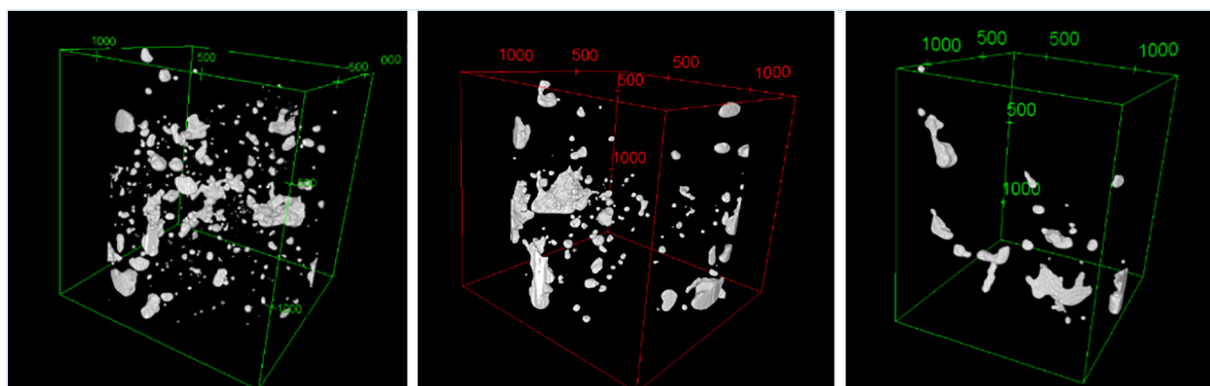


Fig. 2. X-ray images of the gas voids in the same Vāja fiberbank sediment sampled over time (respectively 1, 50 and 109 days since the experimental start, from left to right).

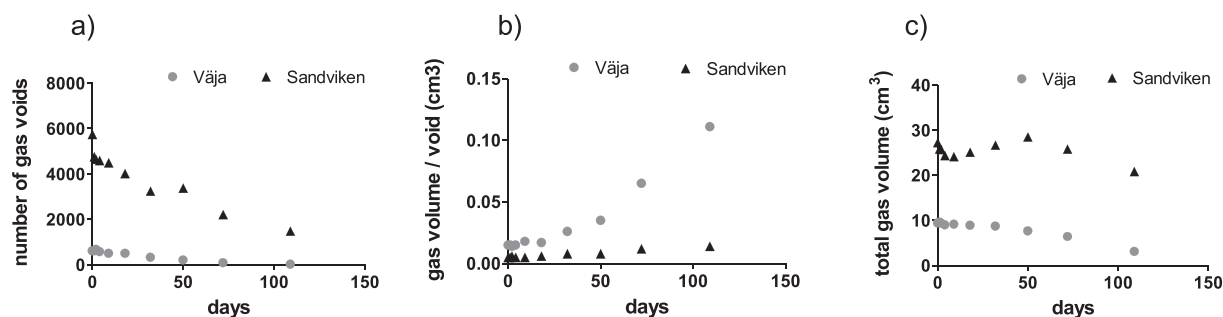


Fig. 3. Gas voids characteristics from both Vāja and Sandviken samples measured over time: number of gas voids (a), average void volume (b), and total gas volume (c).

a decrease after 50 days of experiment. This behavior was not observed in the Vāja column, which instead showed a steady total volume followed by a decrease after 32 days of experiment. This phenomenon can be due to gas accumulation in the sediment, followed by a gas breakthrough, which created channel(s) through the sediment that facilitated subsequent gas release, similar to the pockmarks observed in the field at many fiberbank sites. This observation might have consequences for in-situ remediation methods such as capping, where the protecting capping layer can be disrupted by gas ebullition, therefore affecting its effectiveness.

The increase in average size of the gas voids, together with the decreasing number of gas voids, was observed in both columns and follow a similar trend, albeit to different extents; the Sandviken column shows about three to seven times higher total void volumes than the Vāja column throughout the experiment. The average void volumes being higher in Vāja than in Sandviken (around two to eight times higher), together with the higher number of gas voids in Sandviken, shows that the Sandviken fiberbank sample contains more small voids, whether the Vāja sample contains fewer and larger voids (Figs. 2 and 3).

These void volume measurements reflect the potential of the sediment to entrap the produced gas. It appears that small gas voids remain isolated in Sandviken fiberbanks, whereas in Vāja they merge into bigger ones. As observed by Liu et al. (2018), gas entrapment can be directly linked to the structure of the material; they showed that fine-grained, low shear strength sediments allow for bubble growth. Shear strength measurements are not available for fibrous and heterogeneous materials such as fiberbank sediments. From a qualitative assessment, the fine cellulose fibers from the Vāja fiberbank allow enhanced bubble migration and growth whereas the coarse and chippy Sandviken sediment (which we assume has higher shear strength than Vāja material) restricted such migration. This assessment shows that the findings from Liu et al. (2018) are extendable to fibrous sediments.

The shape of the gas voids observed in the fiberbanks are very different from the disk-shaped bubbles described by Gardiner et al. (2003). The shapes observed are more similar to the spherical or elongated bubbles described by Liu et al. (2018) but with both horizontal and vertical orientations. The results suggest an elastoplastic deformation of the sediment media, which indicates an ability to deform by bubble growth without fracturing, and such deformation can be reversible.

3.2. Gas bubbles released from fiberbanks through ebullition

The results of the optically monitored incubation experiments show that the number of bubbles released, as well as the average gas volume per day, are positively correlated (Spearman's rank correlation coefficient $r = 0.98$, $p < 0.001$) with temperature, for both sediment types (Fig. 4). A significantly higher gas volume was released per day in Vāja ($23 \pm 1.0 \text{ cm}^3/\text{day}$) than in Sandviken ($16 \pm 1.9 \text{ cm}^3/\text{day}$) at 20°C (unpaired t -test, $p < 0.05$). No clear effect of temperature on the bubble size was observed, within the temperature range studied (Fig. S2). The average volume of the gas bubbles released at various temperatures (between 4 and 20°C) was 0.10 cm^3 for Vāja fiberbank and 0.07 cm^3 for Sandviken fiberbank, which explains why the similar measured number of bubbles for both sediments leads to a higher gas volume per day for Vāja. The sizes of released gas bubbles were similar to the size of the gas voids entrapped in the Vāja samples after more than 100 days of monitoring, although gas void sizes continued to increase during the X-ray experiment. In the Sandviken fiberbank samples, the trapped gas voids after 100 days of monitoring were about a quarter of the average size of the released bubbles.

3.3. Gas composition

The composition of the gas collected from both sampled fiberbanks at room temperature showed high concentrations of CH_4 (average 56%

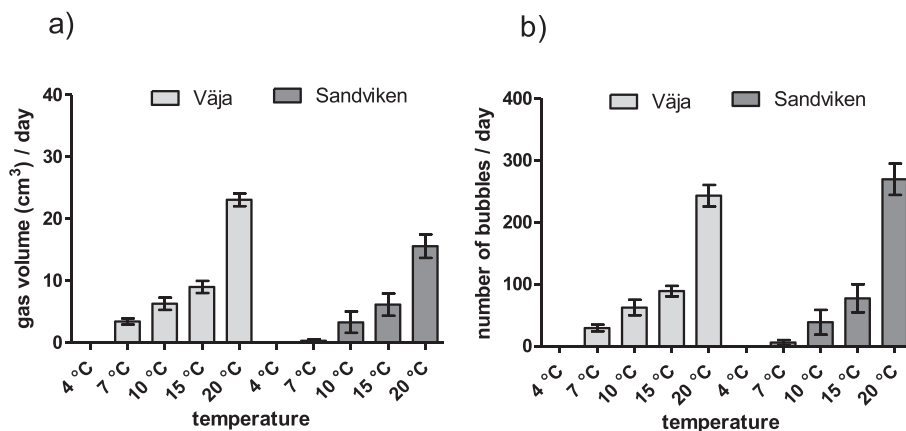


Fig. 4. The volume of gas released per day (a) and the number of gas bubbles released per day (b), during incubation at different temperatures (4°C , 7°C , 10°C , 15°C and 20°C). Data presented as average with error bars showing the standard deviation.

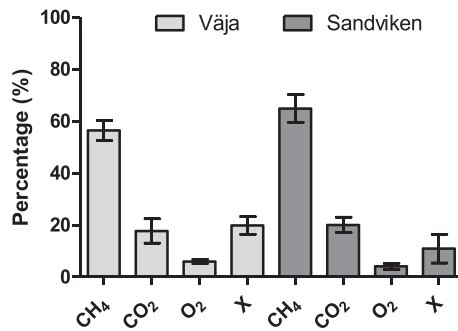


Fig. 5. Composition of the gas produced by fiberbank sediments from Vāja ($n = 3$) and Sandviken ($n = 3$) measured by Biogas 5000 instrument. Data presented as average with error bars showing the standard deviation. X = unidentified gases.

Vāja and 65% Sandviken) and CO₂ (average 18% Vāja and 20% Sandviken) (Fig. 5 and Table S2). Oxygen was also measured (average 6.0% Vāja and 4.1% Sandviken). Since the sediments are anoxic, these oxygen levels can be attributed to air contamination in the experimental setup, for example from the connections between the gas bags and the columns. A large proportion of unidentified gas or gases was also present in the Vāja and Sandviken samples (10% and 20%, respectively). Those are likely nitrogen gas (N₂), detected by complementary Raman spectroscopy measurements and originating at least partly from the previously mentioned air contamination, and other nitrous gases such as N₂O. In addition, hydrogen sulfide (H₂S) was measured in the gas at levels ranging from 0 to 400 ppm using the biogas analyzer. The high CH₄ content is concerning regarding greenhouse gas effects. In comparison, Chatterjee et al. (2018) reported methane contents between 50 and 62% when treating fibrous sediments in biogas reactors.

3.4. Methane production at different temperatures

The CH₄ production in incubated fiberbank samples increases with temperature (Fig. 6 and Table S3). Both types of sediments show a significant log-linear correlation to temperature (Spearman's rank correlation coefficient $r = 1.0$, $p < 0.05$). Vāja fiberbank produced approximately 1.6 times more CH₄ than Sandviken fiberbank at 4.7 °C, and 1.9

times more CH₄ at 20.6 °C. A comparison with literature data (Fig. 6) shows that the CH₄ production from these two fiberbanks is on average about one to three orders of magnitude higher than any (to our knowledge) reported rate from soil or sediment, for any temperature between 4.7 and 20 °C. The measured production rates from fiberbanks follow the same increasing trend with temperature as reported for other sediments. The high CH₄ production rates measured in this study can be attributed to the fiberbanks' high organic content (34–38% TOC, Table S1) compared to the other studies which reported TOC ranging between 1 and 34% (Table S4). The high TOC content and the type of lignocellulose and allochthonous material can be factors that support an extremely active microbial community in fiberbanks compared to other sediment types that contain more natural organic matter. Furthermore, the way in which fiberbank material was deposited on the seafloor is very different from naturally buried organic matter, which usually slowly sinks through the oxygenated water column before it reaches the oxygenated sediment surface, and is already highly degraded before it is buried in anoxic sediment layers. In the case of fiberbanks, however, relatively large amounts of fibrous material were dumped in a relatively short period of time, quickly accumulating on the seafloor and causing anoxic conditions. Hence, this material has undergone little, if any, natural aerobic degradation processes before burial, and is, therefore, likely a better substrate for methanogens than naturally degraded organic matter. Missing information about the microbial communities present in fiberbanks and how they qualitatively and quantitatively differ compared to other gas producing sediments warrants further studies.

Vāja fiberbank sediment showed a significantly higher CH₄ production rate (regression slope elevation, $p < 0.0001$) across the temperature gradient compared to the Sandviken fiberbank sediment (Fig. 6). However, the slightly higher carbon to nitrogen ratio (C/N ratio) measured in Vāja fiberbank (C/N:138) compared to Sandviken (C/N:114, Table S1) would be expected to lead to a slightly lower CH₄ production in Vāja, since relatively more carbon (and higher C/N) is considered to reflect more complex compounds in the organic matter, which are more resistant to degradation (Duarte, 1992; Enriquez et al., 1993; Grasset et al., 2019). Instead, the higher production rate in Vāja is more likely to be due to the finer and processed fibers found at this site that may be quicker to degrade due to the larger surface area accessible for microbial activity, compared to the coarse wood chips found in

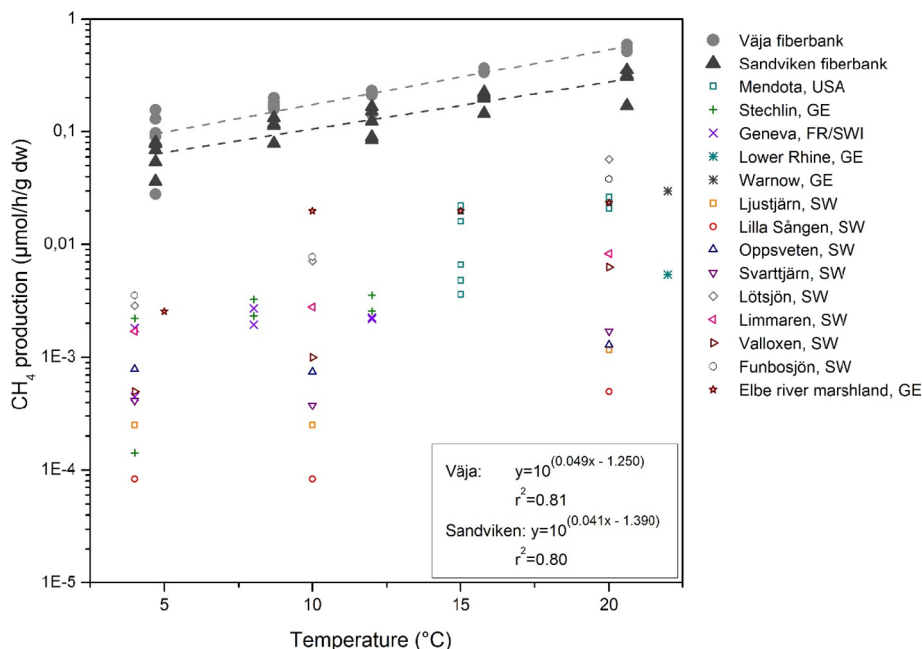


Fig. 6. Methane fluxes from fiberbanks compared with reported fluxes in the literature for soils (Elbe river marshland) and sediments (all others) (Duc et al. (2010), Fuchs et al. (2016), Gebert et al. (2006), Wagner and Pfeiffer (1997), Zeikus and Winfrey (1976)). The dotted lines are fitted to our data according to the equations specified on the figure.

Sandviken fiberbank where plant tissues are bound with cellulose and are inaccessible for microbes.

The used literature data were obtained through similar procedures to allow comparison, and emission rates related to sediment surface area were not considered. Fiberbanks' thickness varies and can be up to several meters (Norrlin and Josefsson, 2017). The influence of the fiberbank thickness might be major considering that this type of sediment is relatively young (<100 years) and accumulated at much higher rates compared to the estuary's deeper sediment accumulation basins. Therefore, the gas production might be similar throughout a whole fiberbank, leading to release rates dependent on sediment thickness.

3.5. Potential methane emission from Swedish fiberbanks

The total volume of fiberbank sediments in Sweden as well as in other countries is unknown. The 39 surveyed sites have a combined estimated total volume of 6,974,000 m³ of fiberbanks, although 336 other sites are likely to contain such sediments, according to their industrial history (Norrlin and Josefsson, 2017). Considering the above-mentioned volumes of sediment found in Sweden, and assuming that similar volumes will be found in the sites that have not yet been fully studied, a potential volume of fiberbanks in Sweden can be estimated to 67,057,697 m³ (considering a total of 375 sites, excluding the 8 sites that have already been remediated). Assuming that the methane and carbon dioxide concentrations and production rates measured in the laboratory at low temperature (4.7 °C) are similar to field production rates for all this volume of fiberbank sediment (average value for both Våja and Sandviken fiberbank of 14.0 and 15.01 µmol/L/h respectively for methane and carbon dioxide), the total fiberbank methane production may reach 1.31×10^5 tons per year, and the carbon dioxide production 3.89×10^5 tons per year. Together, this represents 3.67×10^6 tons CO₂ equivalents per year when using a CH₄ GWP of 25 over 100 years' timescale and only including indirect effects from enhancements of ozone and stratospheric water vapor according to Forster et al. (2007), in order to compare with data from the Swedish EPA, (2020). This production is equivalent to 7% of the estimated total anthropogenic GHG emissions in Sweden in year 2019 (excluding international transports and carbon dioxide uptake) (Swedish-EPA, 2020). However, not all the gas that is potentially produced by fiberbanks is likely to reach the atmosphere. Indeed, part of the methane produced in the sediment is likely to be oxidized once it reaches oxygenated water, for example at the sediment surface (Bastviken, 2009). Moreover, excessive anaerobic organic matter degradation in pulp waste may at some point inhibit further methane production due to the accumulation of by-products such as sulfide, tannins or other organic compounds, and to potential changes in pore water pH that becomes unfavorable for anaerobic degradation (Chen et al., 2008). Finally, the produced gases can be stored in the sediment for undefined periods of time. Despite field observations of gas release (gas ebullition events), no fluxes have yet been measured from fiberbanks.

This study shows that anthropogenic fiberbanks may represent a significant contribution to Sweden's GHG emissions, which should be more precisely quantified and accounted for. Continued surveys of fiberbank sites and gas flux measurements are needed in the first place to refine this estimate calculation from laboratory measurements. These findings stress the need of remediation of these fiberbank sites, to manage not only contaminant dispersal but also to reduce this uncontrolled release of GHG to the atmosphere.

4. Conclusions

The organic-rich fiberbank sediments studied were found to produce extreme amounts of gas within the studied temperature ranges.

The gas formed was partly trapped in the sediment's fibrous structure in small gas voids, expanding and joining together with time. The size of the fibers and wood pieces influenced this process, with a finer structure allowing an easier gas transport and formation of bigger gas voids within the sediment. When the gas exited the sediment, the size of the bubbles was relatively constant over time, although on average smaller in the coarser sediment (Sandviken fiberbanks) than in the finer sediment (Våja fiberbanks). A sharp increase of gas production and release with temperature was also observed. The gas release might induce an enhanced transport of contaminants through gas ebullition, either through bubble migration and/or particle resuspension (Klein, 2006; Yuan et al., 2007). The gas formation may also limit the effectiveness of in-situ remediation techniques, such as for example capping methods (Yuan et al., 2009).

The gas released from the samples from the two fiberbanks had a high content of CH₄ and CO₂, which are both potent GHG. This study shows that the methane production rates are strongly dependent on temperature, and such rates are higher than any previously reported (between 4 and 20 °C). This gas production represents a yet unaccounted source of GHG with potential relevance to global warming. It is therefore important to better evaluate the actual volume of sediment that can be classified as fiberbanks in the aquatic environment around the globe. Our controlled laboratory-scale measurements aimed to understand the field-scale reality that might be observed at various sites presenting such sediments, although actual field results might differ depending on sediment heterogeneities, water depth, waves and currents and other disturbances (e.g. boat traffic). The relationship between fiberbank sediment composition and age/thickness and GHG production and release needs to be further studied and accounted for in order to better assess this source and adjust the predictions accordingly. Our results are concerning in a context of climate change in which the warmer temperatures expected in boreal areas, where forest industries are located, are likely to induce higher GHG emissions from the fiberbanks in the future.

CRedit authorship contribution statement

Alizée P. Lehoux: Conceptualization, Investigation, Visualization, Supervision, Writing – original draft, Writing – review & editing. **Anastasija Isidorova:** Investigation, Writing – review & editing. **Fredrik Collin:** Methodology, Investigation, Writing – review & editing. **John Koestel:** Methodology, Writing – review & editing. **Ian Snowball:** Funding acquisition, Writing – review & editing. **Anna-Karin Dahlberg:** Conceptualization, Investigation, Visualization, Writing – original draft, Writing – review & editing, Funding acquisition.

Declaration of competing interest

The authors declare that they have no known competing financial interests or personal relationships that could have appeared to influence the work reported in this paper.

Acknowledgments

This study is part of the research project GASFIB (project number: 2018-01219), financially supported by The Swedish Research Council for Environment, Agricultural Sciences and Spatial planning (FORMAS).

We would like to acknowledge the crew on SV Ocean Surveyor (Geological Survey of Sweden) for helping us with the field sampling as part of the FIBREM project (VINNOVA, project number: 2016-03337).

A.I. was supported by the European Research Council under the European Union's Seventh Framework Program (FP7/2007–2013)/ERC Grant Agreement 336642.

Appendix A. Supplementary data

Supplementary data to this article can be found online at <https://doi.org/10.1016/j.scitotenv.2021.146772>.

References

- Ali, M., Sreekrishnan, T.R., 2001. Aquatic toxicity from pulp and paper mill effluents: a review. *Adv. Environ. Res.* 5, 175–196. [https://doi.org/10.1016/s1093-0191\(00\)00055-1](https://doi.org/10.1016/s1093-0191(00)00055-1).
- Apler, A., Nyberg, J., Jönsson, K., Hedlund, I., Heinemo, S.-Å., Kjellin, B., 2014. Fiberbanksprojektet - Kartläggning av fiberhaltiga sediment längs Västernorrlands kust. Geological Survey of Sweden, Report no. 2014:16.
- Apler, A., Snowball, I., Frogner-Kockum, P., Josefsson, S., 2019. Distribution and dispersal of metals in contaminated fibrous sediments of industrial origin. *Chemosphere* 215, 470–481. <https://doi.org/10.1016/j.chemosphere.2018.10.010>.
- Apler, A., Snowball, I., Josefsson, S., 2020. Dispersal of cellulose fibers and metals from contaminated sediments of industrial origin in an estuary. *Environ. Pollut.* 266, 115182–115190. <https://doi.org/10.1016/j.envpol.2020.115182>.
- Bastviken, D., 2009. Methane. In: Likens, G. (Ed.), *Encyclopedia of Inland Waters*. Elsevier, Oxford, pp. 783–805.
- Bastviken, D., Cole, J., Pace, M., Tranvik, L., 2004. Methane emissions from lakes: dependence of lake characteristics, two regional assessments, and a global estimate. *Glob. Biogeochem. Cycles* 18. <https://doi.org/10.1029/2004gb002238>.
- Berberich, M.E., Beaulieu, J.J., Hamilton, T.L., Waldo, S., Buffam, I., 2020. Spatial variability of sediment methane production and methanogen communities within a eutrophic reservoir: importance of organic matter source and quantity. *Limnol. Oceanogr.* 65, 1336–1358. <https://doi.org/10.1002/lno.11392>.
- Biberhofer, J., Gauvin, M.A., Prokopec, C.M., 2011. The Geometry and Estimated Volume of Sediment Contained within the Northeast Sector of Thunder Bay Harbour, Thunder Bay, Ontario, National Water Research Institute.
- Chatterjee, P., Lahtinen, L., Kokko, M., Rintala, J., 2018. Remediation of sedimented fiber originating from pulp and paper industry: laboratory scale anaerobic reactor studies and ideas of scaling up. *Water Res.* 143, 209–217. <https://doi.org/10.1016/j.watres.2018.06.054>.
- Chen, Y., Cheng, J.J., Creamer, K.S., 2008. Inhibition of anaerobic digestion process: a review. *Bioresour. Technol.* 99, 4044–4064. <https://doi.org/10.1016/j.biortech.2007.01.057>.
- Dahlberg, A.-K., Apler, A., Vogel, L., Wiberg, K., Josefsson, S., 2020. Persistent organic pollutants in wood fiber-contaminated sediments from the Baltic Sea. *Journal of Soils and Sediments* 20, 2471–2483. <https://doi.org/10.1007/s11368-020-02610-6>.
- Delwiche, K., Hemond, H.F., 2017. An enhanced bubble size sensor for long-term ebullition studies. *Limnology and Oceanography-Methods* 15, 821–835. <https://doi.org/10.1002/lom3.10201>.
- Delwiche, K., Senft-Grupp, S., Hemond, H., 2015. A novel optical sensor designed to measure methane bubble sizes in situ. *Limnology and Oceanography-Methods* 13, 712–721. <https://doi.org/10.1002/lom3.10060>.
- Doube, M., et al., 2010. BoneJ free and extensible bone image analysis in ImageJ. *Bone* 47, 1076–1079. <https://doi.org/10.1016/j.bone.2010.08.023>.
- Duarte, C.M., 1992. Nutrient concentration of aquatic plants - patterns across species. *Limnol. Oceanogr.* 37, 882–889. <https://doi.org/10.4319/lno.1992.37.4.0882>.
- Duc, N.T., Crill, P., Bastviken, D., 2010. Implications of temperature and sediment characteristics on methane formation and oxidation in lake sediments. *Biogeochemistry* 100 (1), 185–196.
- Enriquez, S., Duarte, C.M., Sandjensen, K., 1993. Patterns in decomposition rates among photosynthetic organisms - the importance of detritus C-N-P content. *Oecologia* 94, 457–471. <https://doi.org/10.1007/bf00566960>.
- Fenchel, T., King, G.M., Blackburn, T.H., 2012. *Bacterial metabolism*. In: Third edn (Ed.), *Bacterial Biogeochemistry*. Elsevier Ltd., p. 34.
- Fendinger, N.J., Adams, D.D., Clotfelty, D.E., 1992. The role of gas ebullition in the transport of organic contaminants from sediment. *Sci. Total Environ.* 112, 189–201. [https://doi.org/10.1016/0048-9697\(92\)90187-w](https://doi.org/10.1016/0048-9697(92)90187-w).
- Forster, P., Ramaswamy, V., Artaxo, P., Bernsten, T., Betts, R., Fahey, D.W., Haywood, J., Lean, J., Lowe, D.C., Myhre, G., Nganga, J., Prinn, R., Raga, G., Schulz, M., Van Dorland, R., 2007. Changes in atmospheric constituents and in radiative forcing. In: Solomon, S., Qin, D., Manning, M., Chen, Z., Marquis, M., Averyt, K.B., Tignor, M., Miller, H.L. (Eds.), *Climate Change 2007: The Physical Science Basis. Contribution of Working Group I to the Fourth Assessment Report of the Intergovernmental Panel on Climate Change*. Cambridge University Press, Cambridge, United Kingdom and New York, NY, USA.
- Fuchs, A., Lyautey, E., Montuelle, B., Casper, P., 2016. Effects of increasing temperatures on methane concentrations and methanogenesis during experimental incubation of sediments from oligotrophic and mesotrophic lakes. *Journal of Geophysical Research-Biogeosciences* 121 (5), 1394–1406.
- Gardiner, B.S., Boudreau, B.P., Johnson, B.D., 2003. Growth of disk-shaped bubbles in sediments. *Geochimica Et Cosmochimica Acta* 67, 1485–1494. [https://doi.org/10.1016/s0016-7037\(02\)01072-4](https://doi.org/10.1016/s0016-7037(02)01072-4).
- Gebert, J., Koethe, H., Groengroeft, A., 2006. Prognosis of methane formation by river sediments. *Journal of Soils and Sediments* 6 (2), 75–83.
- Grasset, C., Abril, G., Mendonca, R., Roland, F., Sobek, S., 2019. The transformation of macrophyte-derived organic matter to methane relates to plant water and nutrient contents. *Limnology and Oceanography* 64, 1737–1749. <https://doi.org/10.1002/lno.11148>.
- Johnson, M., Fairweather, M., Harbottle, D., Hunter, T.N., Peakall, J., Biggs, S., 2017. Yield stress dependency on the evolution of bubble populations generated in consolidated soft sediments. *AICHE J.* 63, 3728–3742. <https://doi.org/10.1002/aic.15731>.
- Judd, A.G., Hovland, M., Dimitrov, L.L., Garcia-Gil, S., Jukes, V., 2002. The geological methane budget at continental margins and its influence on climate change. *Geofluids* 2, 109–126. <https://doi.org/10.1046/j.1468-8123.2002.00027.x>.
- Klein, S., 2006. Sediment porewater exchange and solute release during ebullition. *Mar. Chem.* 102, 60–71. <https://doi.org/10.1016/j.marchem.2005.09.014>.
- Koestel, J., 2018. SoilJ: an ImageJ plugin for the semiautomatic processing of three-dimensional X-ray images of soils. *Vadose Zone J.* 17. <https://doi.org/10.2136/vzj2017.03.0062>.
- Kokko, M., Koskue, V., Rintala, J., 2018. Anaerobic digestion of 30–100-year-old boreal lake sedimented fibre from the pulp industry: extrapolating methane production potential to a practical scale. *Water Res.* 133, 218–226.
- Legland, D., Arganda-Carreras, I., Andrey, P., 2016. MorphoLibJ: integrated library and plugins for mathematical morphology with ImageJ. *Bioinformatics* 32, 3532–3534. <https://doi.org/10.1093/bioinformatics/btw413>.
- Liu, L., Wilkinson, J., Koca, K., Buchmann, C., Lorke, A., 2016. The role of sediment structure in gas bubble storage and release. *Journal of Geophysical Research-Biogeosciences* 121, 1992–2005. <https://doi.org/10.1002/2016jg003456>.
- Liu, L., De Kock, T., Wilkinson, J., Cnudde, V., Xiao, S., Buchmann, C., Uteau, D., Peth, S., Lorke, A., 2018. Methane bubble growth and migration in aquatic sediments observed by X-ray μ CT. *Environmental Science & Technology* 52, 2007–2015. <https://doi.org/10.1021/acs.est.7b06061>.
- Myhre, G., Shindell, D., Brön, F.-M., Collins, W., Fuglestedt, J., Huang, J., Koch, D., Lamarque, J.-F., Lee, D., Mendoza, B., Nakajima, T., Robock, A., Stephens, G., Takemura, T., Zhang, H., 2013. Anthropogenic and natural radiative forcing. In: Stocker, T.F., Qin, D., Plattner, G.K., Tignor, M., Allen, S.K., Boschung, J., Nauels, A., Xia, Y., Bex, V., Midgley, P.M. (Eds.), *Climate Change 2013: The Physical Science Basis. Contribution of Working Group I to the Fifth Assessment Report of the Intergovernmental Panel on Climate Change*. Cambridge University Press, Cambridge, United Kingdom and New York, NY, USA, pp. 659–740.
- Norrlin, J., Josefsson, S., 2017. Förorenade fibersediment i svenska hav och sjöar (Geological Survey of Sweden).
- Paranaíba, J.R., et al., 2018. Spatially resolved measurements of CO₂ and CH₄ concentration and gas-exchange velocity highly influence carbon-emission estimates of reservoirs. *Environmental Science & Technology* 52, 607–615. <https://doi.org/10.1021/acs.est.7b05138>.
- Rodríguez, J., Gallampois, C.M.J., Haglund, P., Timonen, S., Rowe, O., 2021. Bacterial communities as indicators of environmental pollution by POPs in marine sediments. *Environ. Pollut.* 268, 115690–115700. <https://doi.org/10.1016/j.envpol.2020.115690>.
- Scandella, B.P., Varadarajan, C., Hemond, H.F., Ruppel, C., Juanes, R., 2011. A conduit dilation model of methane venting from lake sediments. *Geophys. Res. Lett.* 38. <https://doi.org/10.1029/2011gl046768>.
- Scandella, B.P., Delwiche, K., Hemond, H.F., Juanes, R., 2017. Persistence of bubble outlets in soft, methane-generating sediments. *Journal of Geophysical Research-Biogeosciences* 122, 1298–1320. <https://doi.org/10.1002/2016jg003717>.
- Schneider, C.A., Rasband, W.S., Eliceiri, K.W., 2012. NIH image to ImageJ: 25 years of image analysis. *Nat. Methods* 9, 671–675. <https://doi.org/10.1038/nmeth.2089>.
- Swedish-EPA, 2020. Territorial emissions and uptake of greenhouse gases. <http://www.naturvardsverket.se/klimatutslapp> Accessed 2021-03-16.
- Team RC, 2017. R: A Language and Environment for Statistical Computing R Foundation for Statistical Computing, Vienna, Austria.
- van Kessel, T., van Kesteren, W.G.M., 2002. Gas production and transport in artificial sludge depots. *Waste Manag.* 22, 19–28. [https://doi.org/10.1016/s0956-053x\(01\)00021-6](https://doi.org/10.1016/s0956-053x(01)00021-6).
- Viana, Z.P., Yin, K., Rockne, J.K., 2012. Field measurements and modeling of ebullition-facilitated flux of heavy metals and polycyclic aromatic hydrocarbons from sediments to the water column. *Environmental Science and Technology* 46:12046–12054. <https://doi.org/10.1021/es302579e>.
- Wagner, D., Pfeiffer, E.M., 1997. Two temperature optima of methane production in a typical soil of the Elbe river marshland. *FEMS Microbiol. Ecol.* 22 (2), 145–153.
- Weiss, R.F., 1974. Carbon dioxide in water and seawater: the solubility of a non-ideal gas. *Mar. Chem.* 2, 203–215.
- Wiesenburg, D.A., Guinasso, N.L., 1979. Equilibrium solubilities of methane, carbon monoxide, and hydrogen in water and sea-water. *Journal of Chemical and Engineering Data* 24, 356–360. <https://doi.org/10.1021/jc60083a006>.
- WSDE, 2012. Port Angeles Harbour Sediment Characterization Study. Port Angeles, Washington - Sediment Investigation Report. Washington State Department of Ecology.
- Yuan, Q., Valsaraj, T.K., Reible, D.D., Willson, S.C., 2007. A laboratory study of sediment and contaminant release during gas ebullition. *J. Air Waste Manage. Assoc.* 57, 1103–1111. <https://doi.org/10.3155/1047-3289.57.9.1103>.
- Yuan, Q., Valsaraj, T.K., Reible, D.D., 2009. A model for contaminant and sediment transport via gas ebullition through a sediment cap. *Environ. Eng. Sci.* 26, 1381–1391. <https://doi.org/10.1089/ees.2008.0269>.
- Yvon-Durocher, G., Allen, A.P., Bastviken, D., Conrad, R., Gudas, C., St-Pierre, A., Duc, N.T., Giorgio, P.A., 2014. Methane fluxes show consistent temperature dependence across microbial to ecosystem scales. *Nature* 507, 488–491. <https://doi.org/10.1038/nature13164>.
- Zeikus, J.G., Winfrey, M.R., 1976. Temperature limitation of methanogenesis in aquatic sediments. *Appl. Environ. Microbiol.* 31 (1), 99–107.